

March 2010

# Effects of Residue Background Events in Direct Dark Matter Detection Experiments on the Reconstruction of the Velocity Distribution Function of Halo WIMPs

CHUNG-LIN SHAN

*Department of Physics, National Cheng Kung University  
No. 1, University Road, Tainan City 70101, Taiwan, R.O.C.*

*Physics Division, National Center for Theoretical Sciences  
No. 101, Sec. 2, Kuang-Fu Road, Hsinchu City 30013, Taiwan, R.O.C.*

*E-mail: clshan@mail.ncku.edu.tw*

## Abstract

In our earlier work on the development of a model-independent data analysis method for reconstructing the (moments of the) time-averaged one-dimensional velocity distribution function of Weakly Interacting Massive Particles (WIMPs) by using measured recoil energies from direct Dark Matter detection experiments directly, it was assumed that the analyzed data sets are background-free, i.e., all events are WIMP signals. In this article, as a more realistic study, we take into account a fraction of possible residue background events, which pass all discrimination criteria and then mix with other real WIMP-induced events in our data sets. Our simulations show that, for the reconstruction of the one-dimensional WIMP velocity distribution, the maximal acceptable fraction of residue background events in the analyzed data set(s) of  $\mathcal{O}(500)$  total events is  $\sim 10\% - 20\%$ . For a WIMP mass of 50 GeV with a negligible uncertainty and 20% residue background events, the deviation of the reconstructed velocity distribution would in principle be  $\sim 7.5\%$  with a statistical uncertainty of  $\sim 18\%$  ( $\sim 19\%$  for a background-free data set).

# 1 Introduction

Currently, direct Dark Matter detection experiments searching for Weakly Interacting Massive Particles (WIMPs) are one of the promising methods for understanding the nature of Dark Matter and identifying them among new particles produced at colliders as well as reconstructing the (sub)structure of our Galactic halo [1, 2, 3, 4]. In our earlier work [5], we developed methods for reconstructing the (moments of the) time-averaged one-dimensional velocity distribution of halo WIMPs by using (a functional form of) the recoil spectrum as well as the measured recoil energies directly. This analysis requires *no* prior knowledge about the WIMP density near the Earth *nor* about their scattering cross section on nucleus, the unique required information is the mass of incident WIMPs. We therefore turned to also develop the method for determining the WIMP mass model-independently by combining two experimental data sets with two different target nuclei [6, 7].

In the work on the development of these model-independent data analysis procedures by using measured recoil energies from direct detection experiments directly, it was assumed that the analyzed data sets are background-free, i.e., all events are WIMP signals. Active background discrimination techniques should make this condition possible. For example, the ratio of the ionization to recoil energy, the so-called “ionization yield”, used in the CDMS-II experiment provides an event-by-event rejection of electron recoil events to be better than  $10^{-4}$  misidentification [8]. By combining the “phonon pulse timing parameter”, the rejection ability of the misidentified electron recoils (most of them are “surface events” with sufficiently reduced ionization energies) can be improved to be  $< 10^{-6}$  for electron recoils [8]. Moreover, as demonstrated by the CRESST collaboration [9], by means of inserting a scintillating foil, which causes some additional scintillation light for events induced by  $\alpha$ -decay of  $^{210}\text{Po}$  and thus shifts the pulse shapes of these events faster than pulses induced by WIMP interactions in the crystal, the pulse shape discrimination (PSD) technique can then easily distinguish WIMP-induced nuclear recoils from those induced by backgrounds<sup>1</sup>.

However, as the most important issue in all underground experiments, the signal identification ability and possible residue background events which pass all discrimination criteria and then mix with other real WIMP-induced events in our data sets should also be considered. Therefore, in this article, as a more realistic study, we follow our first work on the effects of residue background events on the determination of the WIMP mass [13] and want to study how well we could reconstruct the WIMP velocity distribution model-independently by using “impure” data sets and how “dirty” these data sets could be to be still useful.

The remainder of this article is organized as follows. In Sec. 2 I review the model-independent method for reconstructing the time-averaged one-dimensional velocity distribution function of halo WIMPs by using data from direct detection experiments directly. In Sec. 3 the effects of residue background events in the analyzed data sets on the measured energy spectrum as well as on the reconstructed WIMP mass will briefly be discussed. In Sec. 4 I show numerical results of the reconstructed WIMP velocity distribution by using mixed data sets with different fractions of residue background events based on Monte Carlo simulations. I conclude in Sec. 5. Some technical details will be given in an appendix.

---

<sup>1</sup>For more details about background discrimination techniques and status in currently running and projected direct detection experiments, see e.g., Refs. [10, 11, 12]

## 2 Methods for reconstructing the one-dimensional WIMP velocity distribution function

In this section I review briefly the methods for reconstructing the one-dimensional WIMP velocity distribution function from the recoil spectrum as well as from experimental data directly. Detailed derivations and discussions can be found in Refs. [5, 14].

### 2.1 From the recoil spectrum

The basic expression for the differential event rate for elastic WIMP–nucleus scattering is given by [3]:

$$\frac{dR}{dQ} = \mathcal{A} F^2(Q) \int_{v_{\min}}^{v_{\max}} \left[ \frac{f_1(v)}{v} \right] dv. \quad (1)$$

Here  $R$  is the direct detection event rate, i.e., the number of events per unit time and unit mass of detector material,  $Q$  is the energy deposited in the detector,  $F(Q)$  is the elastic nuclear form factor,  $f_1(v)$  is the one-dimensional velocity distribution function of the WIMPs impinging on the detector,  $v$  is the absolute value of the WIMP velocity in the laboratory frame. The constant coefficient  $\mathcal{A}$  is defined as

$$\mathcal{A} \equiv \frac{\rho_0 \sigma_0}{2m_\chi m_{\text{r,N}}^2}, \quad (2)$$

where  $\rho_0$  is the WIMP density near the Earth and  $\sigma_0$  is the total cross section ignoring the form factor suppression. The reduced mass  $m_{\text{r,N}}$  is defined by

$$m_{\text{r,N}} \equiv \frac{m_\chi m_{\text{N}}}{m_\chi + m_{\text{N}}}, \quad (3)$$

where  $m_\chi$  is the WIMP mass and  $m_{\text{N}}$  that of the target nucleus. Finally,  $v_{\min}$  is the minimal incoming velocity of incident WIMPs that can deposit the energy  $Q$  in the detector:

$$v_{\min} = \alpha \sqrt{Q} \quad (4)$$

with the transformation constant

$$\alpha \equiv \sqrt{\frac{m_{\text{N}}}{2m_{\text{r,N}}^2}}, \quad (5)$$

and  $v_{\max}$  is the maximal WIMP velocity in the Earth's reference frame, which is related to the escape velocity from our Galaxy at the position of the Solar system,  $v_{\text{esc}} \gtrsim 600$  km/s.

In our earlier work [5], it was found that, by using a time-averaged recoil spectrum  $dR/dQ$  and assuming that no directional information exists, the normalized one-dimensional velocity distribution function of incident WIMPs,  $f_1(v)$ , can be solved from Eq. (1) directly as

$$f_1(v) = \mathcal{N} \left\{ -2Q \cdot \frac{d}{dQ} \left[ \frac{1}{F^2(Q)} \left( \frac{dR}{dQ} \right) \right] \right\}_{Q=v^2/\alpha^2}, \quad (6)$$

where the normalization constant  $\mathcal{N}$  is given by

$$\mathcal{N} = \frac{2}{\alpha} \left\{ \int_0^\infty \frac{1}{\sqrt{Q}} \left[ \frac{1}{F^2(Q)} \left( \frac{dR}{dQ} \right) \right] dQ \right\}^{-1}. \quad (7)$$

Here the integral goes over the entire physically allowed range of recoil energies: starting at  $Q = 0$ , and the upper limit of the integral has been written as  $\infty$ . Note that, because  $f_1(v)$  in Eq. (6) is the normalized velocity distribution, the normalization constant  $\mathcal{N}$  here is independent of the constant coefficient  $\mathcal{A}$  defined in Eq. (2). Moreover, as the most important consequence, the velocity distribution function of halo WIMPs reconstructed by Eq. (6) is independent of the local WIMP density  $\rho_0$  as well as of the WIMP–nucleus cross section  $\sigma_0$ . However, as we will see later, not only the overall normalization constant  $\mathcal{N}$  given in Eq. (7), but also the shape of the velocity distribution, through the transformation  $Q = v^2/\alpha^2$  in Eq. (6), depends on the WIMP mass  $m_\chi$  involved in the coefficient  $\alpha$  defined in Eq. (5).

## 2.2 From experimental data directly

In order to use the expressions (6) and (7) for reconstructing  $f_1(v)$ , one needs a functional form for the recoil spectrum  $dR/dQ$ . In practice this requires usually a fit to experimental data. However, data fitting will re-introduce some model dependence and make the error analysis more complicated. Hence, expressions that allow to reconstruct  $f_1(v)$  directly from experimental data (i.e., measured recoil energies) have also been developed [5]. We started by considering experimental data described by

$$Q_n - \frac{b_n}{2} \leq Q_{n,i} \leq Q_n + \frac{b_n}{2}, \quad i = 1, 2, \dots, N_n, \quad n = 1, 2, \dots, B. \quad (8)$$

Here the entire experimental possible energy range between  $Q_{\min}$  and  $Q_{\max}$  has been divided into  $B$  bins with central points  $Q_n$  and widths  $b_n$ . In each bin,  $N_n$  events will be recorded.

As argued in Ref. [5], the statistical uncertainty on the “slope of the recoil spectrum”,

$$\left[ \frac{d}{dQ} \left( \frac{dR}{dQ} \right) \right]_{Q=Q_n},$$

appearing in the expression (6), scales like the bin width to the power  $-1.5$ . In addition, the wider the bin width, the more the recorded events in this bin, and thus the smaller the statistical uncertainty on the estimator of  $[d/dQ (dR/dQ)]_{Q=Q_n}$ . Hence, since the recoil spectrum  $dR/dQ$  is expected to be approximately exponential, in order to approximate the spectrum in a rather wider range, instead of the conventional standard linear approximation, the following *exponential* ansatz for the *measured* recoil spectrum (*before* normalized by the exposure  $\mathcal{E}$ ) in the  $n$ th bin has been introduced [5]:

$$\left( \frac{dR}{dQ} \right)_{\text{expt}, n} \equiv \left( \frac{dR}{dQ} \right)_{\text{expt}, Q \simeq Q_n} \equiv r_n e^{k_n(Q - Q_{s,n})}. \quad (9)$$

Here  $r_n$  is the standard estimator for  $(dR/dQ)_{\text{expt}}$  at  $Q = Q_n$ :

$$r_n = \frac{N_n}{b_n}, \quad (10)$$

$k_n$  is the logarithmic slope of the recoil spectrum in the  $n$ th  $Q$ -bin, which can be computed numerically from the average value of the measured recoil energies in this bin:

$$\overline{Q - Q_n}|_n = \left( \frac{b_n}{2} \right) \coth \left( \frac{k_n b_n}{2} \right) - \frac{1}{k_n}, \quad (11)$$

where

$$\overline{(Q - Q_n)^\lambda}|_n \equiv \frac{1}{N_n} \sum_{i=1}^{N_n} (Q_{n,i} - Q_n)^\lambda. \quad (12)$$

Then the shifted point  $Q_{s,n}$  in the ansatz (9), at which the leading systematic error due to the ansatz is minimal [5], can be estimated by

$$Q_{s,n} = Q_n + \frac{1}{k_n} \ln \left[ \frac{\sinh(k_n b_n/2)}{k_n b_n/2} \right]. \quad (13)$$

Note that  $Q_{s,n}$  differs from the central point of the  $n$ th bin,  $Q_n$ .

Now, substituting the ansatz (9) into Eq. (6) and then letting  $Q = Q_{s,n}$ , we can obtain that

$$f_{1,\text{rec}}(v_{s,n}) = \mathcal{N} \left[ \frac{2Q_{s,n} r_n}{F^2(Q_{s,n})} \right] \left[ \frac{d}{dQ} \ln F^2(Q) \Big|_{Q=Q_{s,n}} - k_n \right]. \quad (14)$$

Here

$$v_{s,n} = \alpha \sqrt{Q_{s,n}}, \quad (15)$$

and the normalization constant  $\mathcal{N}$  given in Eq. (7) can be estimated directly from the data:

$$\mathcal{N} = \frac{2}{\alpha} \left[ \sum_a \frac{1}{\sqrt{Q_a} F^2(Q_a)} \right]^{-1}, \quad (16)$$

where the sum runs over all events in the sample.

## 2.3 Windowing the data set

As mentioned above, the statistical uncertainty on the slope of the recoil spectrum around the central point  $Q_n$ ,  $[d/dQ (dR/dQ)]_{Q \simeq Q_n}$ , is approximately proportional to  $b_n^{-1.5}$ . Thus, in order to reduce the statistical uncertainty on the reconstructed velocity distribution function by Eq. (14), it seems to be better to use large bin width. However, neither the conventional linear approximation:

$$\left( \frac{dR}{dQ} \right)_{\text{expt}, Q=Q_n} = \frac{N_n}{b_n} \quad (17)$$

nor the exponential ansatz given in Eq. (9) can describe the real (but as yet unknown) recoil spectrum exactly. The neglected terms of higher powers of  $Q - Q_n$  could therefore induce some uncontrolled systematic errors which increase with increasing bin width. Moreover, since the number of bins scales inversely with their size, by using large bins we would be able to estimate  $f_1(v)$  only at a small number of velocities. Additionally, once a quite large bin width is used, it would correspondingly lead to a quite large value of the first reconstructible point of  $f_1(v)$ , i.e.,  $f_{1,\text{rec}}(v_{s,1})$ , since the central point  $Q_1$  as well as the shifted point  $Q_{s,1}$  of the first bin would be quite large. Finally, choosing a fixed bin size, as one conventionally does, would let errors on the estimated logarithmic slopes, and hence also on the estimates of  $f_1(v)$ , increase quickly with increasing  $Q$  or  $v$ . This is due to the essentially exponential form of the expected recoil spectrum, which would lead to a quickly falling number of events in equal-sized bins. By some trial-and-error analyses it was found that the errors are roughly equal in all bins if the bin widths increase linearly [5].

Therefore, it has been introduced in Ref. [5] that one can first collect experimental data in relatively small bins and then combining varying numbers of bins into overlapping “windows”. In particular, the first window would be identical with the first bin. One starts by binning the data, as in Eq. (8), where the bin widths satisfy

$$b_n = b_1 + (n-1)\delta, \quad (18)$$

i.e.,

$$Q_n = Q_{\min} + \left(n - \frac{1}{2}\right) b_1 + \left\lfloor \frac{(n-1)^2}{2} \right\rfloor \delta. \quad (19)$$

Here the increment  $\delta$  satisfies

$$\delta = \frac{2}{B(B-1)} (Q_{\max} - Q_{\min} - Bb_1), \quad (20)$$

$B$  being the total number of bins, and  $Q_{(\min, \max)}$  are the experimental minimal and maximal cut-off energies. Assume up to  $n_W$  bins are collected into a window, with smaller windows at the borders of the range of  $Q$ .

In order to distinguish the numbers of bins and windows, hereafter Latin indices  $n, m, \dots$  are used to label bins, and Greek indices  $\mu, \nu, \dots$  to label windows. For  $1 \leq \mu \leq n_W$ , the  $\mu$ th window simply consists of the first  $\mu$  bins; for  $n_W \leq \mu \leq B$ , the  $\mu$ th window consists of bins  $\mu - n_W + 1, \mu - n_W + 2, \dots, \mu$ ; and for  $B \leq \mu \leq B + n_W - 1$ , the  $\mu$ th window consists of the last  $n_W - (\mu - B)$  bins. This can also be described by introducing the indices  $n_{\mu-}$  and  $n_{\mu+}$  which label the first and last bin contributing to the  $\mu$ th window, with

$$n_{\mu-} = \begin{cases} 1, & \text{for } \mu \leq n_W, \\ \mu - n_W + 1, & \text{for } \mu \geq n_W, \end{cases} \quad (21a)$$

and

$$n_{\mu+} = \begin{cases} \mu, & \text{for } \mu \leq B, \\ B, & \text{for } \mu \geq B. \end{cases} \quad (21b)$$

The total number of windows defined through Eqs. (21a) and (21b) is evidently  $W = B + n_W - 1$ , i.e.,  $1 \leq \mu \leq B + n_W - 1$ .

As shown in the previous subsection, the basic observables needed for the reconstruction of  $f_1(v)$  by Eq. (14) are the number of events in the  $n$ th  $Q$ -bin,  $N_n$ , as well as the average value of the measured recoil energies in this bin,  $\overline{Q - Q_n}|_n$ . For a “windowed” data set, one can easily calculate the number of events per window as

$$N_\mu = \sum_{n=n_{\mu-}}^{n_{\mu+}} N_n, \quad (22)$$

as well as the average value of the measured recoil energies

$$\overline{Q - Q_\mu}|_\mu = \frac{1}{N_\mu} \left( \sum_{n=n_{\mu-}}^{n_{\mu+}} N_n \overline{Q}|_n \right) - Q_\mu, \quad (23)$$

where  $Q_\mu$  is the central point of the  $\mu$ th window. The exponential ansatz in Eq. (9) is now assumed to hold over an entire window. We can then estimate the prefactor as

$$r_\mu = \frac{N_\mu}{w_\mu}, \quad (24)$$

$w_\mu$  being the width of the  $\mu$ th window. The logarithmic slope of the recoil spectrum in the  $\mu$ th window,  $k_\mu$ , as well as the shifted point  $Q_{s,\mu}$  (from the central point of each “window”,  $Q_\mu$ ) can be calculated as in Eqs. (11) and (13) with “bin” quantities replaced by “window” quantities. Note that, due to the combination of bins into overlapping windows, these quantities are all

correlated (for  $n_W \neq 1$ ). The expressions for estimating the covariance matrices are given in the appendix.

Finally, the covariance matrix of the estimates of  $f_1(v)$  at adjacent values of  $v_{s,\mu} = \alpha\sqrt{Q_{s,\mu}}$  is given by

$$\begin{aligned} & \text{cov}(f_{1,\text{rec}}(v_{s,\mu}), f_{1,\text{rec}}(v_{s,\nu})) \\ &= \left[ \frac{f_{1,\text{rec}}(v_{s,\mu})f_{1,\text{rec}}(v_{s,\nu})}{r_\mu r_\nu} \right] \text{cov}(r_\mu, r_\nu) + (2\mathcal{N})^2 \left[ \frac{Q_{s,\mu}Q_{s,\nu}r_\mu r_\nu}{F^2(Q_{s,\mu})F^2(Q_{s,\nu})} \right] \text{cov}(k_\mu, k_\nu) \\ & \quad - \mathcal{N} \left\{ \left[ \frac{f_{1,\text{rec}}(v_{s,\mu})}{r_\mu} \right] \left[ \frac{2Q_{s,\nu}r_\nu}{F^2(Q_{s,\nu})} \right] \text{cov}(r_\mu, k_\nu) + (\mu \longleftrightarrow \nu) \right\}. \end{aligned} \quad (25)$$

Note that Eq. (25) should in principle also include contributions involving the statistical error on the estimator for  $\mathcal{N}$  in Eq. (16). However, this error and its correlations with the errors on the  $r_\mu$  and  $k_\mu$  have been found to be negligible compared to the errors included in Eq. (25) [5].

### 3 Effects of residue background events

In this section I first show some numerical results of the energy spectrum of WIMP recoil signals mixed with a few background events. Then I review the effects of residue background events in the analyzed data sets on the reconstruction of the WIMP mass  $m_\chi$ .

For generating WIMP-induced signals, we use the shifted Maxwellian velocity distribution [2, 3, 5]:

$$f_{1,\text{sh}}(v) = \frac{1}{\sqrt{\pi}} \left( \frac{v}{v_e v_0} \right) \left[ e^{-(v-v_e)^2/v_0^2} - e^{-(v+v_e)^2/v_0^2} \right]. \quad (26)$$

Here  $v_0 \simeq 220$  km/s is the orbital velocity of the Sun in the Galactic frame, and  $v_e$  is the Earth's velocity in the Galactic frame [15, 3, 4]<sup>2</sup>:

$$v_e(t) = v_0 \left[ 1.05 + 0.07 \cos \left( \frac{2\pi(t - t_p)}{1 \text{ yr}} \right) \right]; \quad (27)$$

with  $t_p \simeq$  June 2nd is the date on which the velocity of the Earth relative to the WIMP halo is maximal. As a maximal cut-off of the velocity distribution function, the escape velocity has been set as  $v_{\text{esc}} = 700$  km/s. The Woods-Saxon elastic nuclear form factor [16, 3, 4] for the SI WIMP-nucleus cross section will also be used<sup>3</sup>.

Meanwhile, we use the target-dependent exponential form introduced in Ref. [13] for the residue background spectrum:

$$\left( \frac{dR}{dQ} \right)_{\text{bg,ex}} = \exp \left( -\frac{Q/\text{keV}}{A^{0.6}} \right). \quad (28)$$

Here  $Q$  is the recoil energy,  $A$  is the atomic mass number of the target nucleus. The power index of  $A$ , 0.6, is an empirical constant, which has been chosen so that the exponential background spectrum is somehow similar to, but still different from the expected recoil spectrum of the target nuclei; otherwise, there is in practice no difference between the WIMP scattering and background

<sup>2</sup>The time dependence of the Earth's velocity in the Galactic frame, the second term of  $v_e(t)$ , will be ignored in our simulations, i.e.,  $v_e = 1.05 v_0$  will be used.

<sup>3</sup>Other commonly used analytic forms for the one-dimensional WIMP velocity distribution as well as for the elastic nuclear form factor for the SI WIMP-nucleus cross section can be found in Refs. [5, 17].

spectra. Note that, among different possible choices, we use in our simulations the atomic mass number  $A$  as the simplest, unique characteristic parameter in the general analytic form (28) for defining the residue background spectrum for different target nuclei. However, it does not mean that the (superposition of the real) background spectra would depend simply/primarily on  $A$  or on the mass of the target nucleus,  $m_N$ . In other words, it is practically equivalent to use expression (28) or  $(dR/dQ)_{\text{bg,ex}} = e^{-Q/13.5 \text{ keV}}$  directly for a  $^{76}\text{Ge}$  target.

Note also that, firstly, as argued in Ref. [13], the exponential form of background spectrum is rather naive; but, since we consider here only *a few (tens) residue* background events induced by perhaps *two or more* different sources, pass all discrimination criteria, and then mix with other WIMP-induced events in our data sets of a few hundreds *total* events, exact forms of different background spectra are actually not very important and this exponential form should practically not be unrealistic<sup>4</sup>. Secondly, as demonstrated in Ref. [5] and reviewed in the previous section, the model-independent data analysis procedure for reconstructing the WIMP velocity distribution function requires only measured recoil energies (induced mostly by WIMPs and occasionally by background sources) from direct detection experiments. Therefore, for applying this method to future real data, a prior knowledge about (different) background source(s) is *not required at all*.

Moreover, for our numerical simulations presented here as well as in the next section, the actual numbers of signal and background events in each simulated experiment are Poisson-distributed around their expectation values *independently*; and the total event number recorded in one experiment is then the sum of these two numbers. Additionally, we assumed that all experimental systematic uncertainties as well as the uncertainty on the measurement of the recoil energy could be ignored. The energy resolution of most existing detectors is so good that its error can be neglected compared to the statistical uncertainty for the foreseeable future with pretty few events.

### 3.1 On the measured energy spectrum

In Figs. 1 I show measured energy spectra (solid red histograms) for a  $^{76}\text{Ge}$  target with six different WIMP masses: 10, 25, 50, 100, 250, and 500 GeV based on Monte Carlo simulations. The dotted blue curves are the elastic WIMP-nucleus scattering spectra, whereas the dashed green curves are the exponential background spectra given in Eq. (28), which have been normalized so that the ratios of the areas under these background spectra to those under the (dotted blue) WIMP scattering spectra are equal to the background-signal ratio in the whole data sets (e.g., 20% backgrounds to 80% signals shown in Figs. 1). The experimental threshold energy has been assumed to be negligible and the maximal cut-off energy is set as 100 keV. The background windows (the possible energy ranges in which residue background events exist) have been assumed to be the same as the experimental possible energy ranges. 5,000 experiments with 500 total events on average in each experiment have been simulated. Remind that the measured energy spectra shown here are averaged over the simulated experiments. Five bins with linear increased bin widths have been used for binning generated signal and background events. As argued in Sec. 2.3, for reconstructing the one-dimensional WIMP velocity distribution function, this unusual, particular binning has been chosen in order to accumulate more events in high energy ranges and thus to reduce the statistical uncertainties in high velocity ranges.

It can be found in Figs. 1 that, the shape of the WIMP scattering spectrum depends highly on the WIMP mass: for light WIMPs ( $m_\chi \lesssim 50 \text{ GeV}$ ), the recoil spectra drop sharply with increasing

---

<sup>4</sup>Other (more realistic) forms for background spectrum (perhaps also for some specified targets/experiments) can be tested on the AMIDAS website [18, 19].



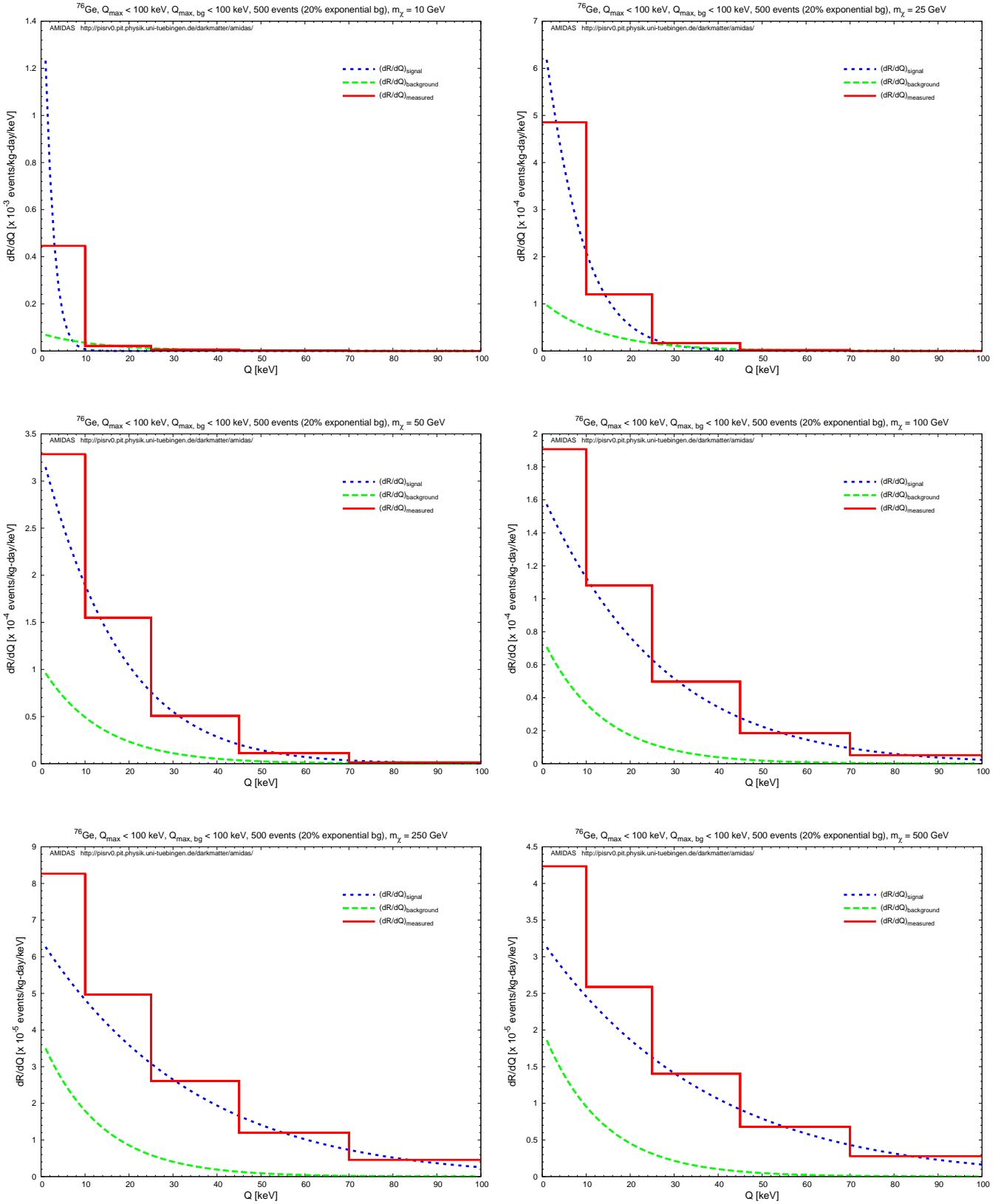


Figure 1: Measured energy spectra (solid red histograms) for a  $^{76}\text{Ge}$  target with six different WIMP masses: 10, 25, 50, 100, 250, and 500 GeV. The dotted blue curves are the elastic WIMP–nucleus scattering spectra, whereas the dashed green curves are the exponential background spectra normalized to fit to the chosen background ratio, which has been set as 20% here. The experimental threshold energy has been assumed to be negligible and the maximal cut–off energy is set as 100 keV. The background windows have been assumed to be the same as the experimental possible energy ranges. 5,000 experiments with 500 total events on average in each experiment have been simulated. See the text for further details (plots from Ref. [13]).

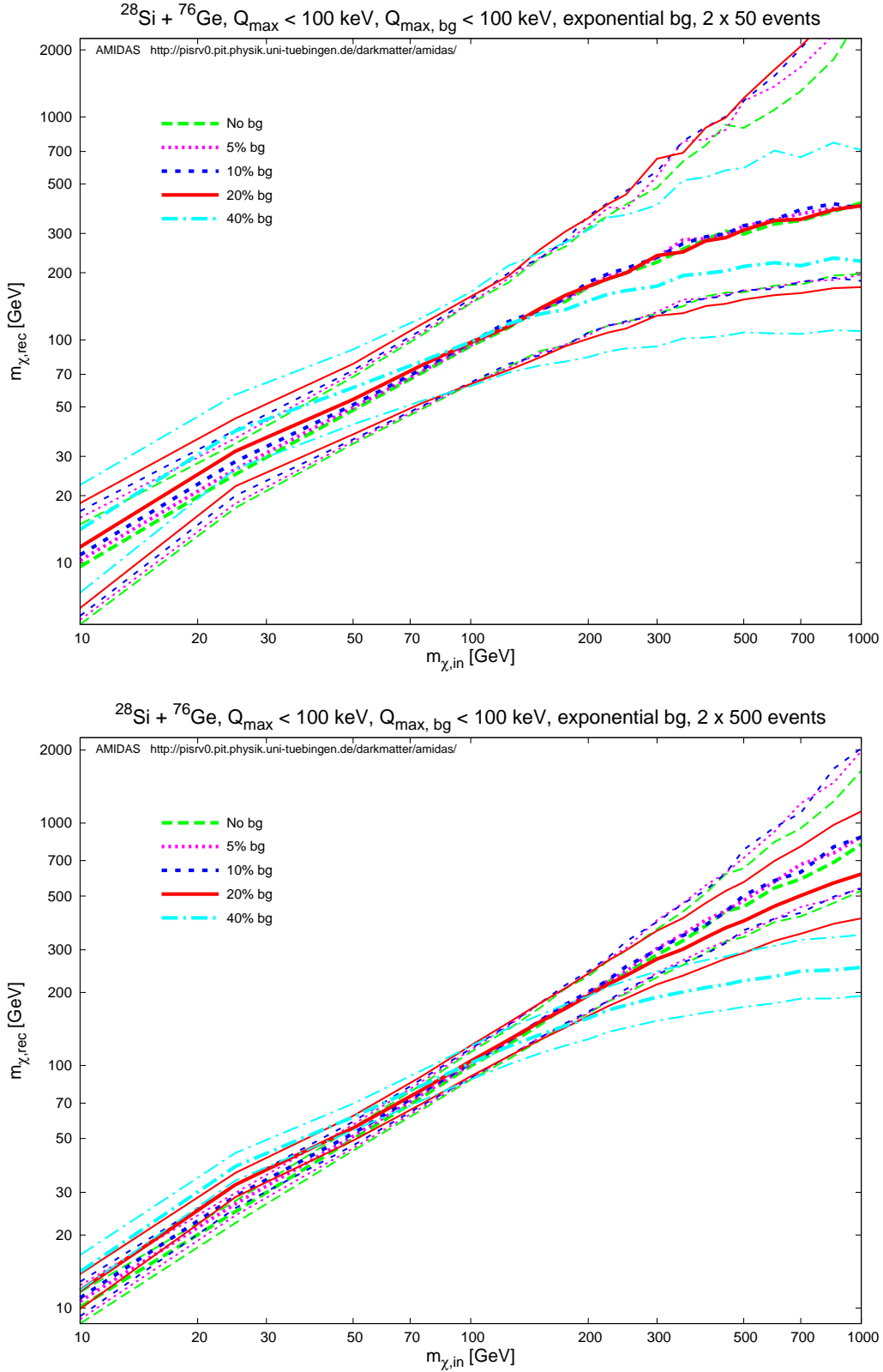


Figure 2: The reconstructed WIMP mass and the lower and upper bounds of the  $1\sigma$  statistical uncertainty by using mixed data sets from WIMP-induced and background events as functions of the input WIMP mass.  $^{28}\text{Si}$  and  $^{76}\text{Ge}$  have been chosen as two target nuclei. The background ratios shown here are no background (dashed green curves), 5% (dotted magenta curves), 10% (long-dotted blue curves), 20% (solid red curves), and 40% (dash-dotted cyan curves) background events in the analyzed data sets in the experimental energy ranges between 0 and 100 keV. Each experiment contains 50 (upper) and 500 (lower) total events on average. Other parameters are as in Figs. 1. See the text for further details.

recoil energies, while for heavy WIMPs ( $m_\chi \gtrsim 100$  GeV), the spectra become flatter. In contrast, the exponential background spectra shown here depend only on the target mass and are rather flatter (sharper) for light (heavy) WIMP masses compared to the WIMP scattering spectra. This means that, once input WIMPs are light (heavy), background events would contribute relatively more to high (low) energy ranges, and, consequently, the measured energy spectra would mimic scattering spectra induced by heavier (lighter) WIMPs.

More detailed illustrations and discussions about the effects of residue background events on the measured energy spectrum can be found in Ref. [13].

### 3.2 On the reconstructed WIMP mass

Figs. 2 show the reconstructed WIMP mass and the lower and upper bounds of the  $1\sigma$  statistical uncertainty by means of the model-independent procedure introduced in Refs. [6, 7] with mixed data sets from WIMP-induced and background events as functions of the input WIMP mass. As in Ref. [7],  $^{28}\text{Si}$  and  $^{76}\text{Ge}$  have been chosen as two target nuclei. The experimental threshold energies of two experiments have been assumed to be negligible and the maximal cut-off energies are set the same as 100 keV. The background windows are set as the same as the experimental possible energy ranges for both experiments. The background ratios shown here are no background (dashed green curves), 5% (dotted magenta curves), 10% (long-dotted blue curves), 20% (solid red curves), and 40% (dash-dotted cyan curves) background events in the analyzed data sets.  $2 \times 5,000$  experiments have been simulated. Each experiment contains 50 (upper) and 500 (lower) total events on average. Note that *all* events recorded in our data sets are treated as WIMP signals in the analysis, although statistically we know that a fraction of these events could be backgrounds.

It can be seen clearly that, for light WIMP masses ( $m_\chi \lesssim 100$  GeV), due to the relatively flatter background spectrum (compared to the scattering spectrum induced by light WIMPs), the energy spectrum of all recorded events would mimic a scattering spectrum induced by WIMPs with a relatively heavier mass, and, consequently, the reconstructed WIMP masses as well as the statistical uncertainty intervals could be overestimated. In contrast, for heavy WIMP masses ( $m_\chi \gtrsim 100$  GeV), due to the relatively sharper background spectrum, relatively more background events contribute to low energy ranges, and the energy spectrum of all recorded events would mimic a scattering spectrum induced by WIMPs with a relatively lighter mass. Hence, the reconstructed WIMP masses as well as the statistical uncertainty intervals could be underestimated. Moreover, Figs. 2 show that the larger the fraction of background events in the data sets, the more strongly over-/underestimated the reconstructed WIMP masses as well as the statistical uncertainty intervals. Nevertheless, from Figs. 2 it can be found that, with  $\sim 10\%$  residue background events in the analyzed data sets of  $\sim 500$  total events, one could still estimate the WIMP mass pretty well; if WIMPs are light ( $m_\chi \lesssim 200$  GeV), the maximal acceptable fraction of residue background events could even be as large as  $\sim 20\%$ .

More detailed illustrations and discussions about the effects of residue background events on the determination of the WIMP mass can be found in Ref. [13].

## 4 Results of the reconstructed one-dimensional WIMP velocity distribution function

In this section I present simulation results of the reconstructed one-dimensional velocity distribution function of halo WIMPs with mixed data sets from WIMP-induced and background

events by means of the model-independent method described in Sec. 2.<sup>5</sup> The WIMP mass  $m_\chi$  involved in the coefficient  $\alpha$  in Eqs. (15) and (16) for estimating the reconstructed points  $v_{s,n}$  (or  $v_{s,\mu}$  for a windowed data set) as well as the normalization constant  $\mathcal{N}$  has been assumed to be known precisely with a negligible uncertainty from other (e.g., collider) experiments or can be determined from *other* direct detection experiments. As in Ref. [5], a  $^{76}\text{Ge}$  nucleus has been chosen as our detector target for reconstructing  $f_1(v)$ ; while a  $^{28}\text{Si}$  target and a *second*  $^{76}\text{Ge}$  target have been used for determining  $m_\chi$ . The experimental threshold energy of each experiment has been assumed to be negligible and the maximal cut-off energies are set the same as 100 keV. The exponential background spectrum given in Eq. (28) has been used for generating background events in windows of the entire experimental possible ranges. As in Figs. 1, five bins have been used<sup>6</sup> and up to three bins have been combined to a window.  $(3 \times) 5,000$  experiments have been simulated.

## 4.1 With a precisely known WIMP mass

In this subsection we first assume that the required WIMP mass for determining the shape of the reconstructed velocity distribution through the transformation (15) from  $Q_{s,n}$  to  $v_{s,n}$  (or from  $Q_{s,\mu}$  to  $v_{s,\mu}$ ) and for estimating the normalization constant  $\mathcal{N}$  by Eq. (16) has been known precisely with a negligible uncertainty.

Figs. 3 show the one-dimensional WIMP velocity distribution function reconstructed by Eq. (14) with data sets of 500 total events on average for six different WIMP masses: 10, 25, 50, 100, 250, and 500 GeV; all events in the data sets are treated as WIMP signals. The vertical error bars show the square roots of the diagonal entries of the covariance matrix<sup>7</sup> given in Eq. (25), while the horizontal bars show the sizes of the windows used for estimating  $f_{1,\text{rec}}(v_{s,\mu})$ . The background ratios shown here are no background (dashed green lines), 10% (long-dotted blue lines), and 20% (solid red lines) background events in the analyzed data set in the background window of the entire experimental possible energy range. Note that, since the experimental maximal cut-off energy is fixed as 100 keV, for heavier input WIMP masses ( $m_\chi \gtrsim 250$  GeV), one can reconstruct the velocity distribution function only in the velocity range  $v \lesssim 300$  km/s.

It can be seen that, as shown in Figs. 1, for heavier WIMP masses ( $m_\chi \gtrsim 100$  GeV), the relatively sharper background spectrum contributes more events to low energy ranges, or, equivalently, to low velocity ranges. This shifts the reconstructed velocity distribution to *lower* velocities. For an input WIMP mass of 100 GeV and the background ratio of 10% (20%), the peak of the reconstructed velocity distribution function could be shifted by 30 (60) km/s.

In contrast, for lighter WIMP masses ( $m_\chi \lesssim 50$  GeV), the relatively flatter background spectrum contributes more events to high energy/velocity ranges. This shifts the reconstructed velocity distribution to *higher* velocities. Note that, however, compared to the cases with the heavy WIMP masses, the reconstructed velocity distribution for light WIMPs seems not to be shifted to higher velocities very much. This should mainly be due to the exponential form of the background spectrum: its contribution to high energy ranges for light WIMPs is relatively not so significant as that to low ranges for heavy WIMPs (see Figs. 1). One exception should be the case with the input WIMP mass of 10 GeV. For this case, the WIMP scattering spectrum drops very sharp in the energy range between 0 and 10 keV, while the exponential background

<sup>5</sup>Note that, rather than the mean values, the (bounds on the) reconstructed  $f_{1,\text{rec}}(v_{s,\mu})$  are always the median values of the simulated results.

<sup>6</sup>For the input WIMP masses of 10 (25) GeV, the widths of the first bin have been modified to 1.5 (5) keV due to a kinematic maximal cut-off energy discussed later.

<sup>7</sup>Remind that, since the neighboring windows overlap, the estimates of  $f_1$  by Eq. (14) at adjacent values of  $v_{s,\mu}$  are correlated.

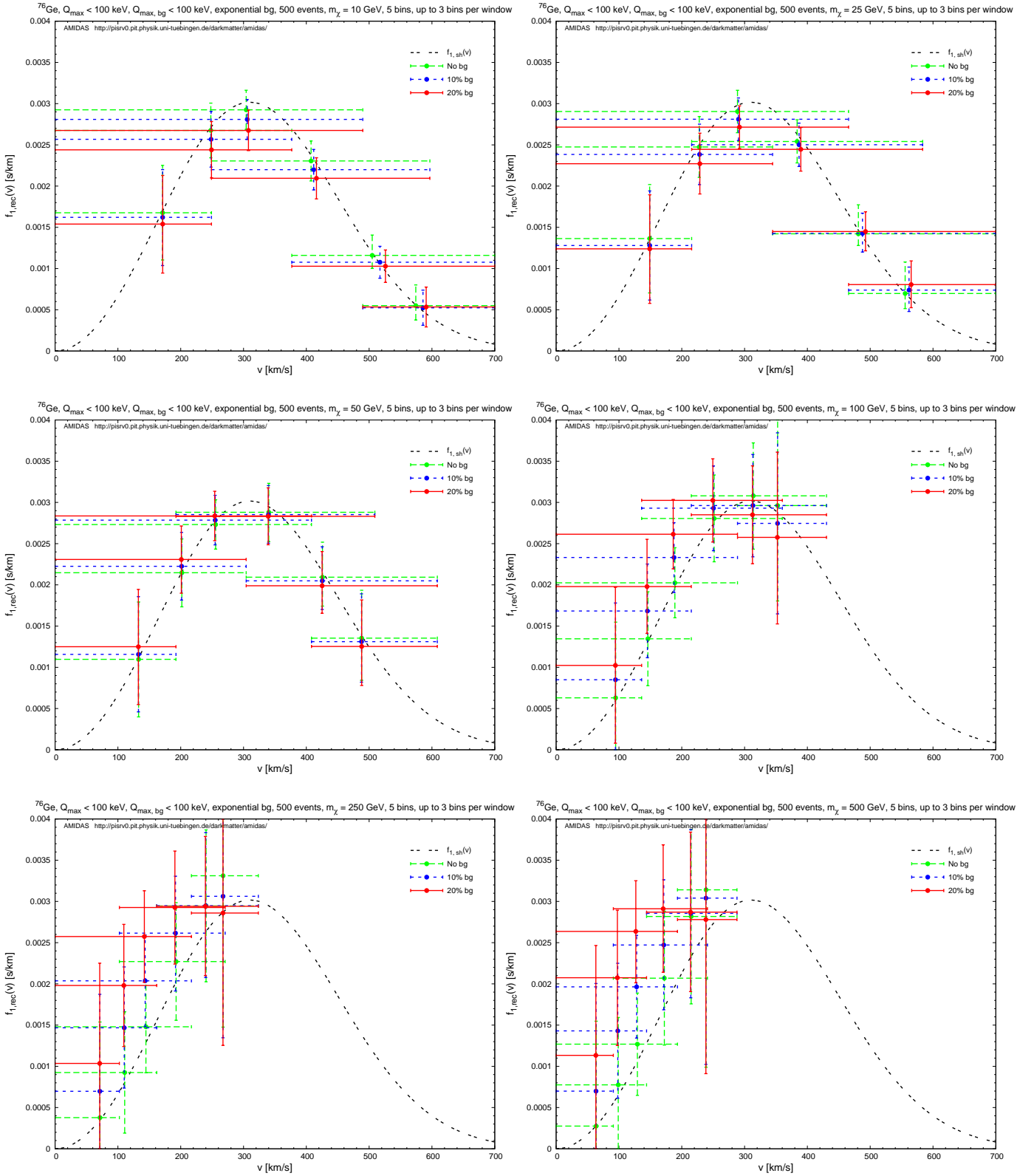


Figure 3: The one-dimensional WIMP velocity distribution function reconstructed by Eq. (14) for six different WIMP masses: 10, 25, 50, 100, 250, and 500 GeV. The double-dotted black curves are the input shifted Maxwellian velocity distribution in Eq. (26). The vertical error bars show the square roots of the diagonal entries of the covariance matrix given in Eq. (25), while the horizontal bars show the sizes of the windows used for estimating  $f_{1,rec}(v_{s,\mu})$ . The background ratios shown here are no background (dashed green lines), 10% (long-dotted blue lines), and 20% (solid red lines) background events in the analyzed data set in the background window of the entire experimental possible energy range. Parameters and notations are as in Figs. 2. See the text for further details.

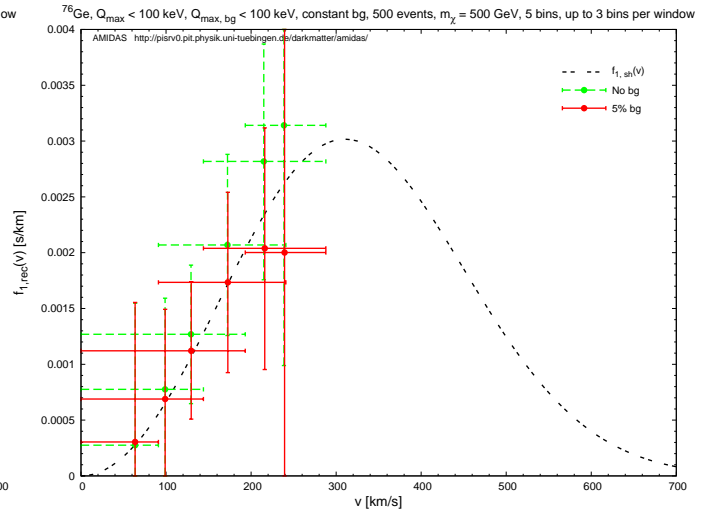
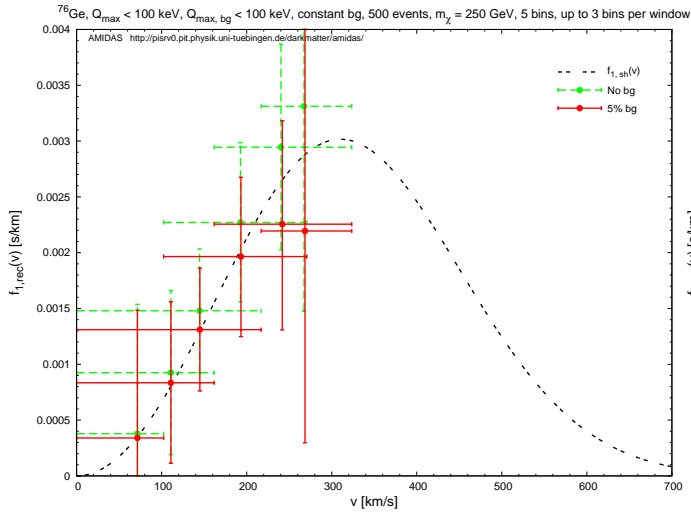
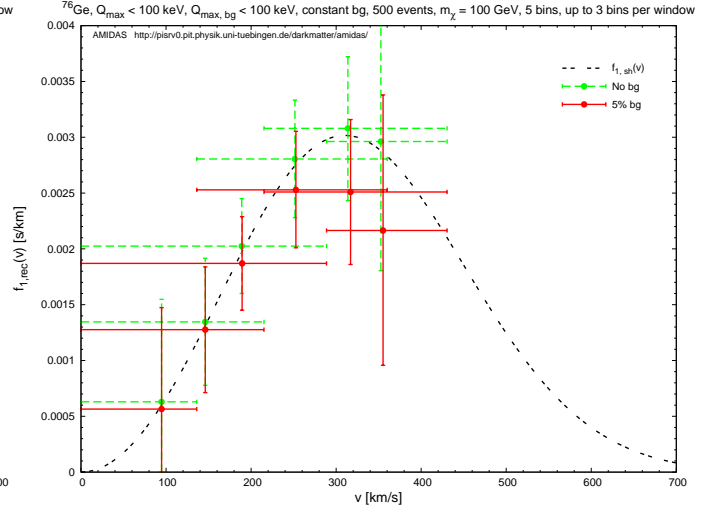
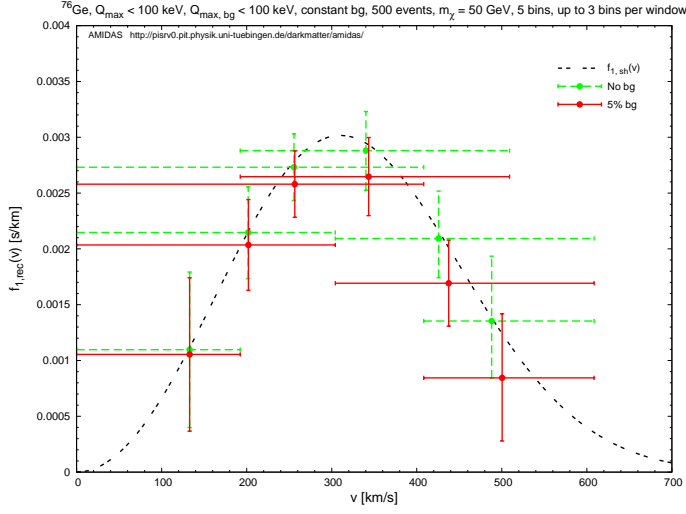
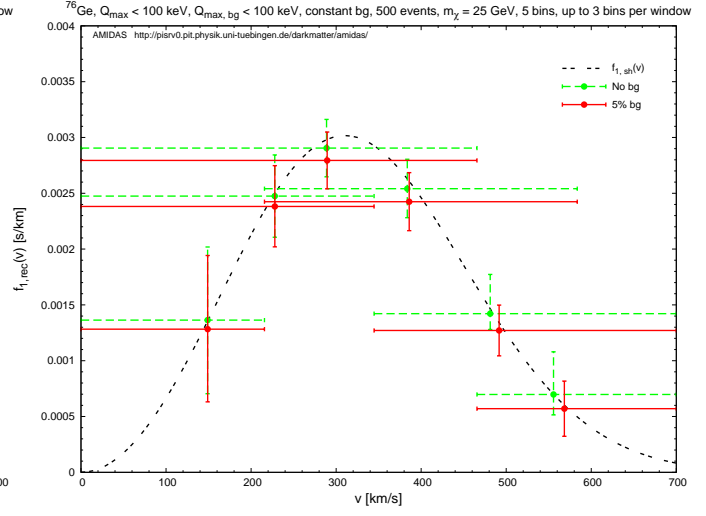
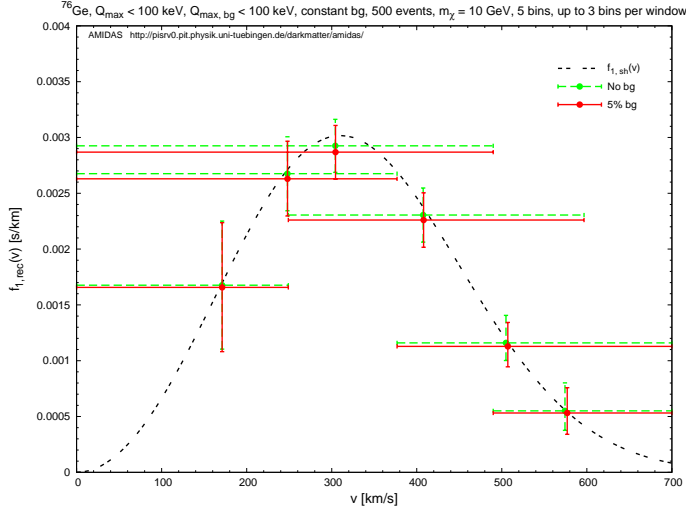


Figure 4: As in Figs. 3, except that the constant background spectrum in Eq. (30) has been used. Note that the solid red lines here indicate a background ratio of 5%.

spectrum extends much wider to 100 keV (see Figs. 1). Thus a large part of background events contribute to energy ranges higher than 10 keV. However, because we reconstruct the WIMP velocity distribution only in the velocity range below the maximal cut-off velocity, i.e., the Galactic escape velocity  $v_{\text{esc}}$ , this leads to a kinematic maximal cut-off of the recoil energy

$$Q_{\text{max,kin}} = \frac{v_{\text{esc}}^2}{\alpha^2}. \quad (29)$$

For a WIMP mass of 10 GeV and a  $^{76}\text{Ge}$  target, it can be calculated that  $Q_{\text{max,kin}} = 11.8$  keV. Therefore, all background events with energies larger than  $\sim 12$  keV have actually been neglected in the data analysis.

Not surprisingly, the larger the background ratio of our data set, the higher/lower the velocities to which the reconstructed velocity distribution will be shifted. But, our simulation results shown in Figs. 3 indicate that, with an  $\sim 10\% - 20\%$  background ratio (i.e.,  $\sim 50 - 100$  events) in the analyzed data set of  $\sim 500$  total events, one could in principle still reconstruct the one-dimensional velocity distribution function of halo WIMPs with an  $\sim 6.5\%$  (for a 25 GeV WIMP mass, 20% background events) –  $\sim 38\%$  (for a 250 GeV WIMP mass, 10% background events) deviation. If the mass of halo WIMPs is  $\mathcal{O}(50 \text{ GeV})$ , the maximal acceptable background ratio could even be as large as  $\sim 40\%$  ( $\sim 200$  events) with a deviation of only  $\sim 14\%$ .

In order to check the need of a prior knowledge about an (exact) form of the residue background spectrum, in Figs. 4 we consider a rather extrem form for the residue background spectrum, i.e., the constant spectrum introduced in Ref. [13]:

$$\left(\frac{dR}{dQ}\right)_{\text{bg,const}} = 1. \quad (30)$$

Here we show only results with a background ratio of 5% (solid red lines). It can be seen clearly that, although a constant background spectrum contributes (much) more events in high energy ranges for all six input WIMP masses<sup>8</sup>, taking into account the pretty large statistical uncertainty, we could at least give a rough outline of the WIMP velocity distribution for heavy WIMP masses ( $m_\chi \gtrsim 100 \text{ GeV}$ ), or even reconstruct the distribution pretty well for light WIMPs ( $m_\chi \lesssim 100 \text{ GeV}$ ), thanks to the kinetic maximal cut-off energy  $Q_{\text{max,kin}}$  discussed above.

## 4.2 With a reconstructed WIMP mass

In this subsection, the required WIMP mass for estimating the reconstructed points  $v_{s,\mu}$  as well as the normalization constant  $\mathcal{N}$  by Eqs. (15) and (16) has been reconstructed with other direct detection experiments<sup>9</sup>. Note that the statistical uncertainty on  $f_{1,\text{rec}}(v_{s,\mu})$  estimated as the diagonal entries of the covariance matrix given in Eq. (25) must thus be modified by taking into account the statistical uncertainty on the reconstructed WIMP mass  $\sigma(m_\chi)$  to

$$\sigma^2(f_{1,\text{rec}}(v_{s,\mu})) = \text{cov}(f_{1,\text{rec}}(v_{s,\mu}), f_{1,\text{rec}}(v_{s,\mu})) + \frac{m_N}{2} \left[ \frac{f_{1,\text{rec}}(v_{s,\mu})}{\alpha m_\chi^2} \right]^2 \sigma^2(m_\chi). \quad (31)$$

In Figs. 5 I show the numerical results with six different input WIMP masses, as shown in Figs. 3. Note that, while the vertical bars show the  $1\sigma$  statistical uncertainties estimated by Eq. (31),

<sup>8</sup>Illustrations and detailed discussions about the effects of the constant form of the residue background spectrum on the measured energy spectrum for different input WIMP masses can be found in Ref. [13].

<sup>9</sup>In order to avoid calculations of the correlations between  $m_\chi$  and  $f_{1,\text{rec}}(v_{s,\mu})$ , we have assumed here that the two data sets using Ge detectors are independent of each other.

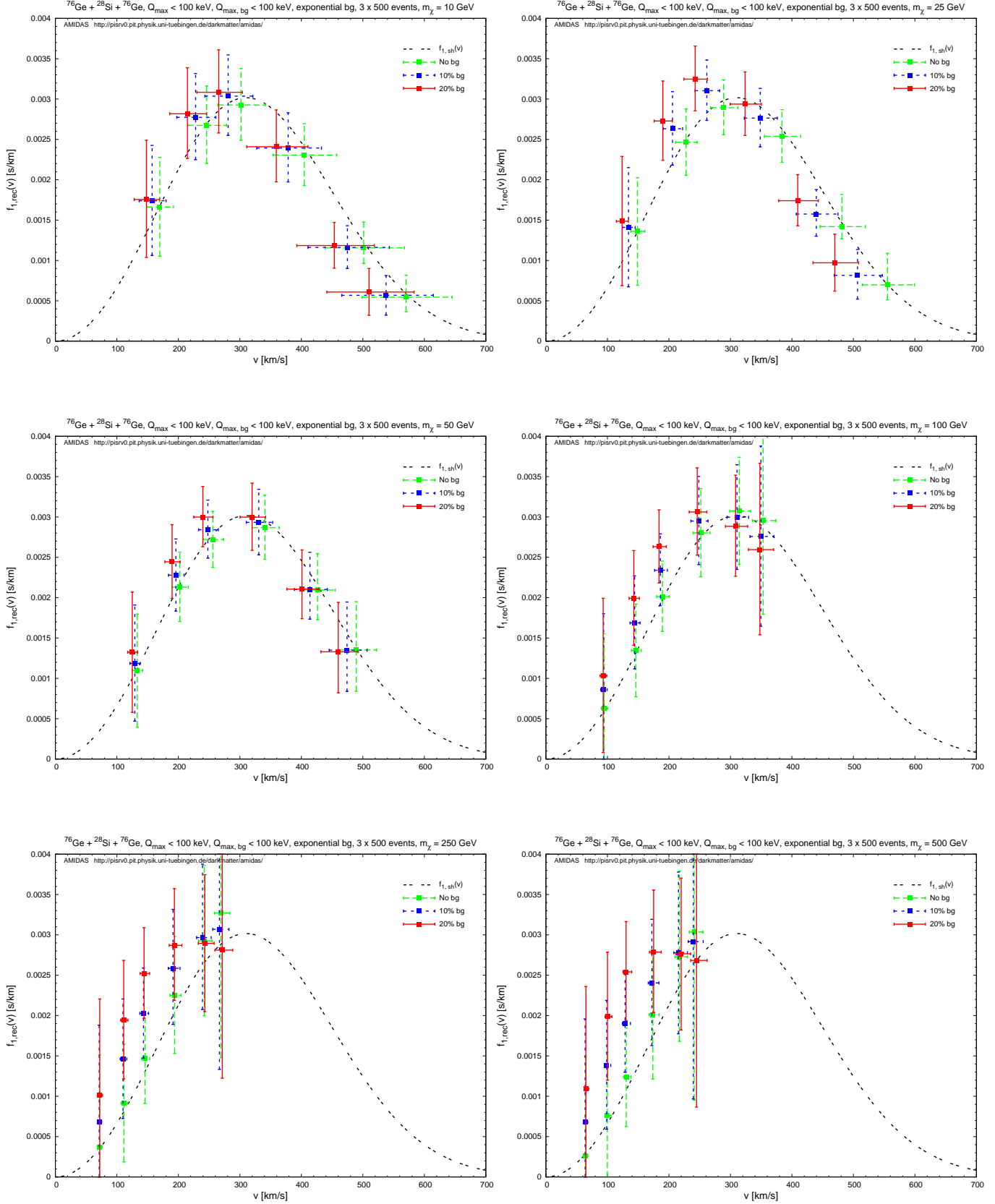


Figure 5: As in Figs. 3, except that the WIMP masses have been reconstructed by means of the procedure introduced in Refs. [6, 7]. Here the vertical bars show the  $1\sigma$  statistical uncertainties estimated by Eq. (31), while the horizontal bars show the  $1\sigma$  statistical uncertainties on the estimates of  $v_{s,\mu}$  given in Eq. (15) due to the uncertainty on the reconstructed WIMP mass. See the text for further details.



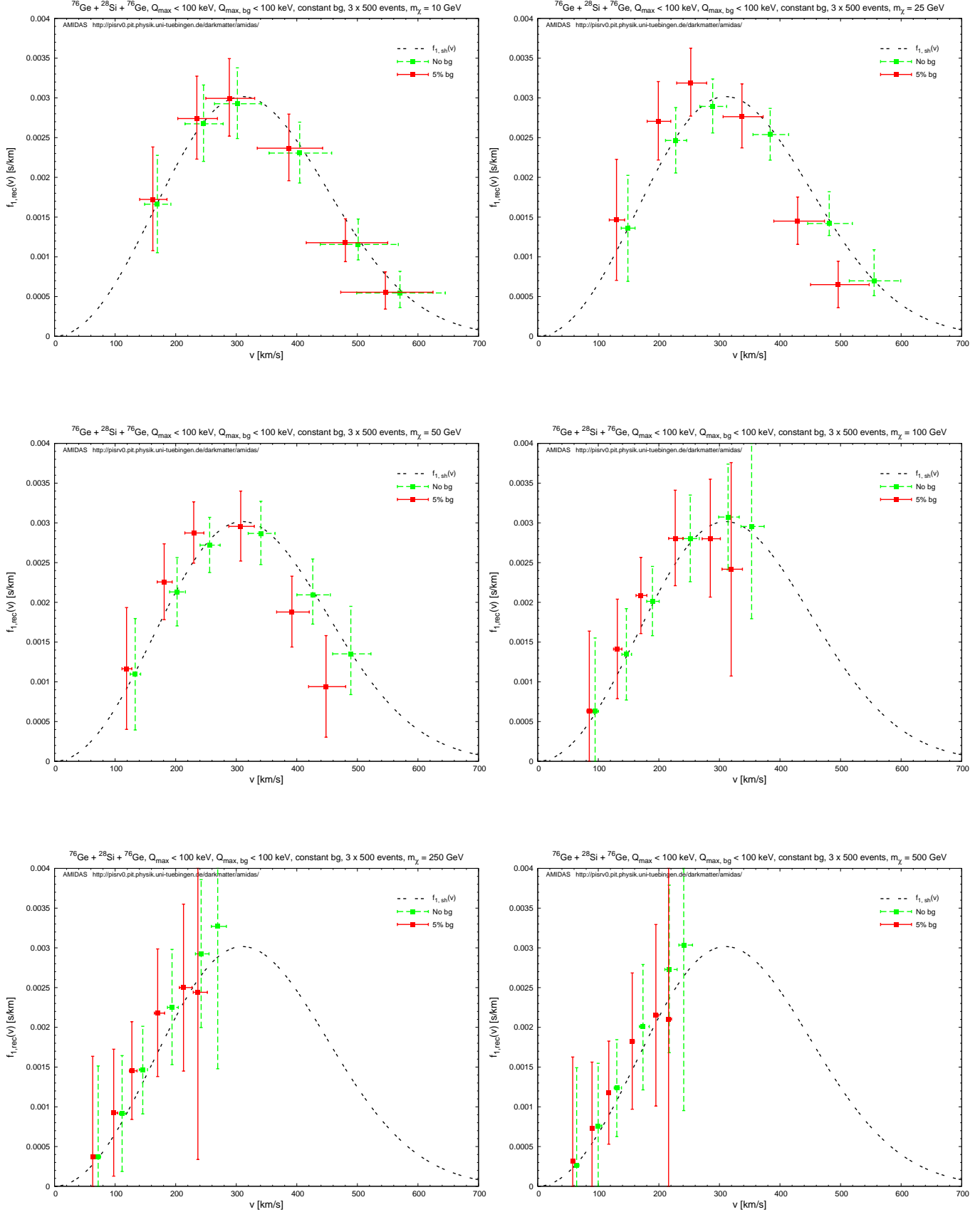


Figure 6: As in Figs. 5, except that the constant background spectrum in Eq. (30) has been used. Note that the solid red lines here indicate a background ratio of 5%.

the horizontal bars shown here indicate the  $1\sigma$  statistical uncertainties on the estimates of  $v_{s,\mu}$  given in Eq. (15) due to the uncertainty on the reconstructed WIMP mass; the statistical and systematic uncertainties due to estimating of  $Q_{s,\mu}$  have been neglected here.

It can be seen that, firstly, as shown in Figs. 2, for an input WIMP mass of 100 GeV, the reconstructed mass doesn't differ very much from the true value. Hence, the reconstructed  $f_{1,\text{rec}}(v_{s,\mu})$  is approximately the same for both cases with the input/reconstructed WIMP mass. However, for light input masses ( $m_\chi \lesssim 100$  GeV), the reconstructed  $f_{1,\text{rec}}(v_{s,\mu})$  with the reconstructed WIMP mass shift to relatively *lower* velocities compared to the case with the input (true) WIMP mass. This effect caused directly by the overestimate of the reconstructed WIMP mass. The coefficient  $\alpha$  defined in Eq. (5) can be rewritten as

$$\alpha = \frac{1}{\sqrt{2m_N}} \left( 1 + \frac{m_N}{m_\chi} \right). \quad (32)$$

This implies that, once the reconstructed WIMP mass is over-/underestimated from the real value, the coefficient  $\alpha$  will thus be under-/overestimated. Consequently,  $v_{s,\mu}$  determined by Eq. (15) will be smaller/larger than the true values.

Note that, firstly, this second effect, in contrast to the first one discussed in the previous subsection, draws the reconstructed WIMP velocity distribution to the opposite directions; i.e., to *lower/higher* velocities if WIMPs are *light/heavy*. Secondly, for heavier WIMP masses, as shown in Figs. 2, with a small background fraction, the underestimate of the reconstructed WIMP mass and thus the shift of the velocity distribution function seem not to be significant. Nevertheless, the simulation results shown in Figs. 5 indicate that, with an  $\sim 5\% - 10\%$  background ratio (i.e.,  $\sim 25 - 50$  events) in the analyzed data sets of  $\sim 500$  total events, one could in principle still reconstruct the one-dimensional velocity distribution function of halo WIMPs with an  $\sim 7\%$  (for 25 GeV WIMPs, 10% backgrounds) –  $\sim 16\%$  (for 250 GeV WIMPs, 5% backgrounds) deviation<sup>10</sup>. If the mass of WIMPs is light ( $m_\chi \lesssim 100$  GeV), the maximal acceptable background ratio could even be as large as  $\sim 20\%$  ( $\sim 100$  events) with a deviation of only  $\sim 9\%$ .

In Figs. 6 we again use the constant spectrum for residue backgrounds and the WIMP mass has been reconstructed by using other mixed data sets. For this case, as shown in Ref. [13], the WIMP mass would be overestimated for all input masses. And, consequently, the reconstructed WIMP velocity distribution for all six input masses are shifted to lower velocity ranges. Nevertheless, as for the case with a known WIMP mass shown in Figs. 4, data sets with background fractions of  $\lesssim 5\%$  could in principle be used to at least give a rough outline of the WIMP velocity distribution (for  $m_\chi \gtrsim 100$  GeV), or even reconstruct the distribution pretty well (for  $m_\chi \lesssim 100$  GeV).

Finally, we rise the expected event number in each experiment a factor of 10, to 5,000 events totally. The experimental maximal cut-off energies for WIMP signals and background windows have also been extended to 150 keV. Nine bins have been used<sup>11</sup> and up to four bins have been combined to a window. Since with  $2 \times 5,000$  events we could in principle determine the WIMP mass with an uncertainty of  $\lesssim 5\%$ , I show only the results of the reconstructed WIMP velocity distribution function with the input WIMP mass in Figs. 7. It can be seen clearly that, by using a data set of  $\mathcal{O}(5,000)$  events with a maximal background ratio of  $\lesssim 5\%$  ( $\mathcal{O}(250)$  events), we could in principle reconstruct the WIMP velocity distribution function in the velocity range

<sup>10</sup>Remind that, as shown in the lower frame of Figs. 2, with two data sets of  $\sim 500$  total events each and a background ratio of  $\sim 10\%$ , the WIMP mass could in principle be reconstructed with a statistical uncertainty of  $\sim 10\%$  (for 25 GeV WIMPs) –  $\sim 25\%$  (for 250 GeV WIMPs).

<sup>11</sup>For the input WIMP masses of 10/25/50 GeV, the widths of the first bin have been set as 1.5/2.5/2.5 keV.

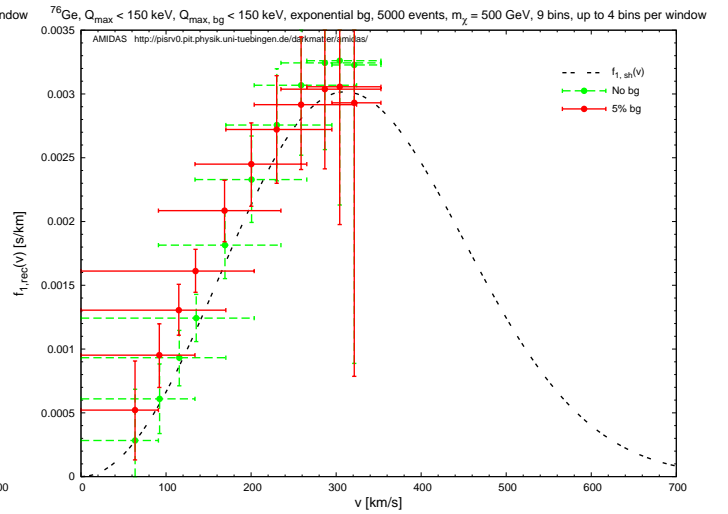
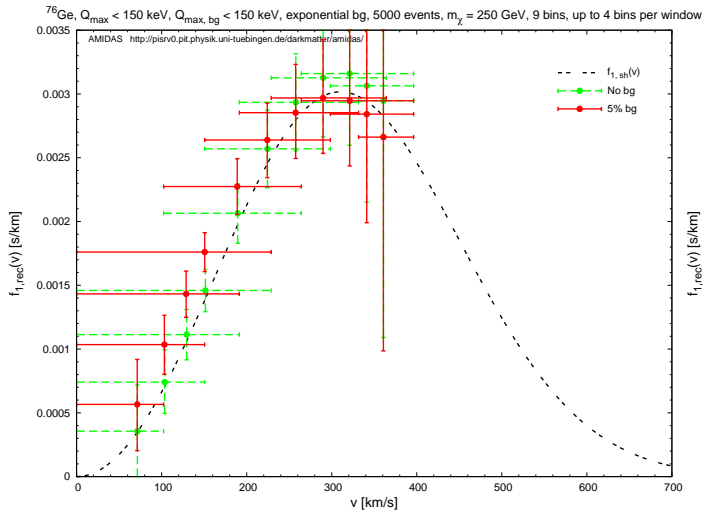
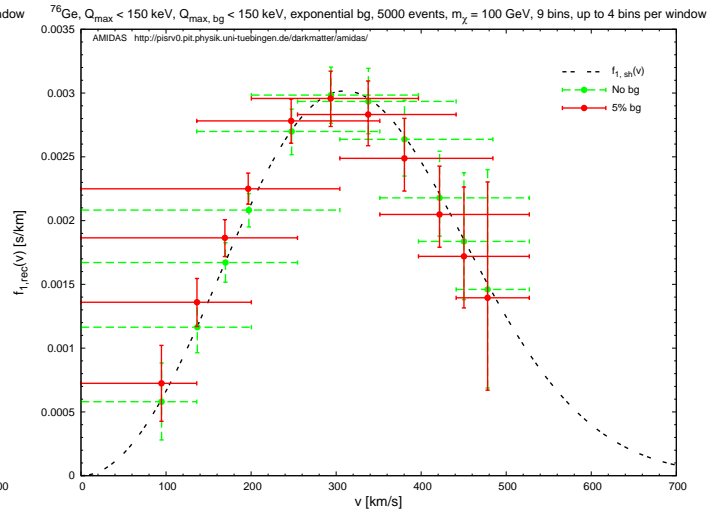
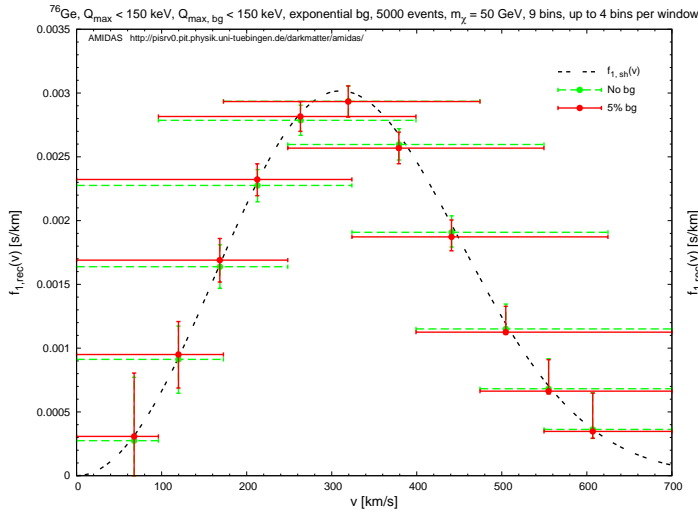
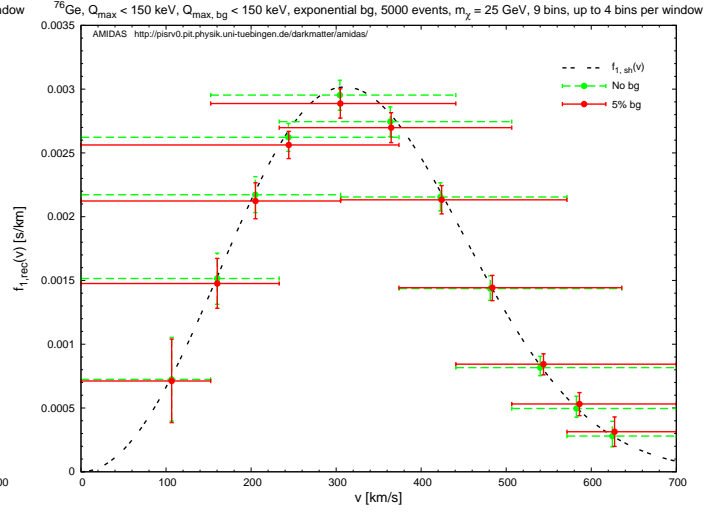
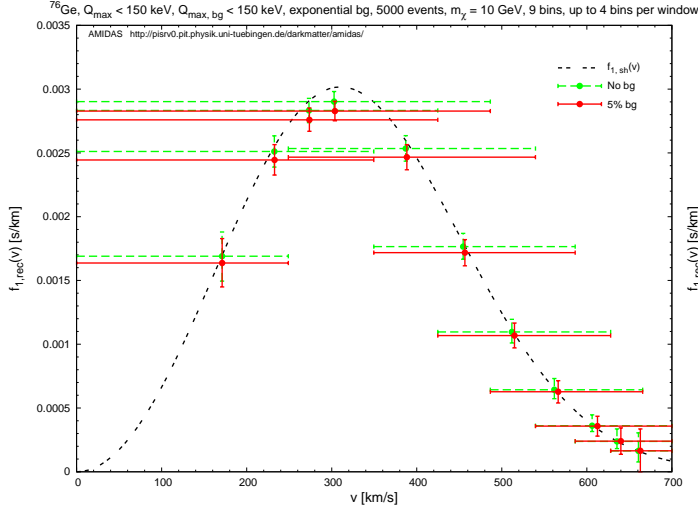


Figure 7: As in Figs. 3, except that the expected number of total events in each experiment has been risen to 5,000 and the experimental maximal cut-off energies for WIMP signals and background windows have been extended to 150 keV. Note that the solid red lines here indicate a background ratio of 5%.

$v \lesssim \mathcal{O}(500 \text{ km/s})$  with a deviation of  $\lesssim 6\%$  (for a WIMP mass of 100 GeV). Once WIMPs are light ( $m_\chi \lesssim \mathcal{O}(50 \text{ GeV})$ ), this deviation could even be reduced to  $\lesssim 2.5\%$ .

## 5 Summary and conclusions

In this paper we reexamine the model-independent data analysis method introduced in Ref. [5] for the reconstruction of the one-dimensional velocity distribution function of Weakly Interacting Massive Particles from data (measured recoil energies) of direct Dark Matter detection experiments directly by taking into account a fraction of residue background events, which pass all discrimination criteria and then mix with other real WIMP-induced events in the analyzed data sets. This method requires neither prior knowledge about the WIMP scattering spectrum nor about different possible background spectra; the unique needed information is the recoil energies recorded in direct detection experiments and (eventually) the mass of incident WIMPs.

For the mass of incident WIMPs required as an unique input information in this method, we first assumed that it could be known precisely with a negligible uncertainty from other (e.g., collider) experiments. Our simulations show that, assuming an exponential form for the residue background spectrum, with a data set of  $\sim 500$  total events, and a background ratio of  $\sim 10\% - 20\%$ , the WIMP velocity distribution function could in principle be reconstructed with an  $\sim 6.5\%$  (for a 25 GeV WIMP mass, 20% background events) –  $\sim 38\%$  (for a 250 GeV WIMP mass, 10% background events) deviation. If the WIMP mass is  $\mathcal{O}(50 \text{ GeV})$ , the maximal acceptable background ratio could be risen to  $\sim 40\%$  with a deviation of only  $\sim 14\%$ .

Moreover, for lighter/heavier WIMP masses, since the relatively flatter/sharper background spectrum could contribute relatively more events to high/low energy ranges, the reconstructed velocity distribution could therefore be shifted to higher/lower velocities. However, since for (very) light WIMPs ( $m_\chi \lesssim 40 \text{ GeV}$ ), the kinematic maximal cut-off of the recoil energy due to the Galactic escape velocity is (much) lower than the experimental cut-off, a (large) fraction of background events in high energy ranges could thus in practice be neglected, and the shift could not be very significant for WIMPs lighter than  $\sim 50 \text{ GeV}$ .

Since a model-independent method for determining the WIMP mass by using two experimental data sets with two different target nuclei has also been developed [6, 7], we considered in this paper also the case that the velocity distribution function is reconstructed with a reconstructed WIMP mass from other direct detection experiments. Our simulations show that, since lighter/heavier WIMP masses could be over-/underestimated by using this method with background-mixed data sets [13], the reconstructed points of the velocity distribution would thus be shifted to lower/higher velocities, the opposite direction of the shift due purely to the background contribution to high/low energy ranges. Although this second effect shifts the reconstructed velocity distribution (much) more strongly, with  $\sim 5\% - 10\%$  background events mixed in the analyzed data sets, the WIMP velocity distribution function could in principle still be reconstructed with an  $\sim 7\%$  (for 25 GeV WIMPs, 10% backgrounds) –  $\sim 16\%$  (for 250 GeV WIMPs, 5% backgrounds) deviation. If the WIMP mass is  $\lesssim \mathcal{O}(100 \text{ GeV})$ , the maximal acceptable background ratio could even be as large as  $\sim 20\%$  with a deviation of only  $\sim 9\%$ .

Furthermore, in order to check the need of a prior knowledge about an (exact) form of the residue background spectrum, a constant spectrum for residue backgrounds has also been considered. Since the WIMP mass would always be overestimated [13], the reconstructed WIMP velocity distribution could thus be (strongly) shifted to lower velocity ranges. However, data sets with background fractions of  $\lesssim 5\%$  could in principle be used to at least give a rough outline of the WIMP velocity distribution (for  $m_\chi \gtrsim 100 \text{ GeV}$ ), or even reconstruct the distribution

pretty well (for  $m_\chi \lesssim 100$  GeV).

Finally, for rather next-to-next generation detectors, we considered also the case of 5,000 total events and extended the maximal experimental cut-off energies for WIMP signals and backgrounds to 150 keV. Assuming a maximal background ratio of  $\lesssim 5\%$ , our results show that the WIMP velocity distribution function could in principle be reconstructed in the velocity range  $v \lesssim \mathcal{O}(500 \text{ km/s})$  with a deviation of  $\lesssim 6\%$  (for a WIMP mass of 100 GeV). Once WIMPs are light ( $m_\chi \lesssim \mathcal{O}(50 \text{ GeV})$ ), this deviation could even be reduced to  $\lesssim 2.5\%$ .

In summary, as the second part of the study of the effects of residue background events in direct Dark Matter detection experiments, we considered the reconstruction of the velocity distribution function of halo WIMPs. Our results show that, with projected experiments using next-generation detectors with  $10^{-9}$  to  $10^{-11}$  pb sensitivities [20, 21, 10, 22] and  $< 10^{-6}$  background rejection ability [9, 11, 12, 8], once one or more experiments with different target nuclei could accumulate a few hundreds events (in one experiment), we could in principle at least give a rough outline of the WIMP velocity distribution function, e.g., an approximate estimate of the location of its peak, even though there could be some background events mixed in our data sets for the analysis. After that, by means of increased number of observed (WIMP-induced) events and improved background discrimination techniques [9, 11], the shape and properties of the velocity distribution of halo Dark Matter should be understood more clearly.

## Acknowledgments

The author would like to thank the Physikalisches Institut der Universität Tübingen for the technical support of the computational work demonstrated in this article. The author would also like to thank the friendly hospitality of the Max-Planck-Institut für Kernphysik in Heidelberg where part of this work was completed. This work was partially supported by the National Science Council of R.O.C. under contract no. NSC-98-2811-M-006-044 as well as by the Focus Group on Cosmology and Particle Astrophysics, National Center of Theoretical Sciences, R.O.C..

## A Formulae needed in Sec. 2

Here I list all formulae needed for the model-independent method described in Sec. 2. Detailed derivations and discussions can be found in Refs. [5, 14].

First, by using the standard Gaussian error propagation, the expression for the error on the logarithmic slope  $k_n$  can be given from Eq. (11) directly as

$$\sigma^2(k_n) = k_n^4 \left\{ 1 - \left[ \frac{k_n b_n / 2}{\sinh(k_n b_n / 2)} \right]^2 \right\}^{-2} \sigma^2(\overline{Q - Q_n|_n}), \quad (\text{A1})$$

with

$$\sigma^2(\overline{Q - Q_n|_n}) = \frac{1}{N_n - 1} \left[ \overline{(Q - Q_n)^2|_n} - \overline{Q - Q_n|_n}^2 \right]. \quad (\text{A2})$$

For replacing the “bin” quantities by “window” quantities, one needs the covariance matrix for  $\overline{Q - Q_\mu|_\mu}$ , which follows directly from the definition (23):

$$\begin{aligned} & \text{cov}(\overline{Q - Q_\mu|_\mu}, \overline{Q - Q_\nu|_\nu}) \\ &= \frac{1}{N_\mu N_\nu} \sum_{n=n_{\nu-}}^{n_{\mu+}} \left[ N_n (\overline{Q|_n} - \overline{Q|_\mu}) (\overline{Q|_n} - \overline{Q|_\nu}) + N_n^2 \sigma^2(\overline{Q - Q_n|_n}) \right]. \end{aligned} \quad (\text{A3})$$

Note that, firstly,  $\mu \leq \nu$  has been assumed here and the covariance matrix is, of course, symmetric. Secondly, the sum is understood to vanish if the two windows  $\mu, \nu$  do not overlap, i.e., if  $n_{\mu+} < n_{\nu-}$ . Moreover, from Eq. (24), we can get

$$\text{cov}(r_\mu, r_\nu) = \frac{1}{w_\mu w_\nu} \sum_{n=n_{\nu-}}^{n_{\mu+}} N_n, \quad (\text{A4})$$

where  $\mu \leq \nu$  has again been taken. And the mixed covariance matrix can be given by

$$\text{cov}\left(r_\mu, \overline{Q - Q_\nu}|_\nu\right) = \frac{1}{w_\mu N_\nu} \sum_{n=n_-}^{n_+} N_n \left(\overline{Q}|_n - \overline{Q}|_\nu\right). \quad (\text{A5})$$

Note here that this sub-matrix is *not* symmetric under the exchange of  $\mu$  and  $\nu$ . In the definition of  $n_-$  and  $n_+$  we therefore have to distinguish two cases:

$$\begin{aligned} n_- = n_{\nu-}, \quad n_+ = n_{\mu+}, & \quad \text{if } \mu \leq \nu; \\ n_- = n_{\mu-}, \quad n_+ = n_{\nu+}, & \quad \text{if } \mu \geq \nu. \end{aligned} \quad (\text{A6})$$

As before, the sum in Eq. (A5) is understood to vanish if  $n_- > n_+$ .

Furthermore, the covariance matrices involving the estimators of the logarithmic slopes  $k_\mu$ , estimated by Eq. (11) with replacing  $n \rightarrow \mu$ , can be given from Eq. (A1) as

$$\begin{aligned} \text{cov}(k_\mu, k_\nu) = k_\mu^2 k_\nu^2 & \left\{ 1 - \left[ \frac{k_\mu b_\mu/2}{\sinh(k_\mu b_\mu/2)} \right]^2 \right\}^{-1} \left\{ 1 - \left[ \frac{k_\nu b_\nu/2}{\sinh(k_\nu b_\nu/2)} \right]^2 \right\}^{-1} \\ & \times \text{cov}\left(\overline{Q - Q_\mu}|_\mu, \overline{Q - Q_\nu}|_\nu\right), \end{aligned} \quad (\text{A7})$$

and

$$\text{cov}(r_\mu, k_\nu) = k_\nu^2 \left\{ 1 - \left[ \frac{k_\nu b_\nu/2}{\sinh(k_\nu b_\nu/2)} \right]^2 \right\}^{-1} \text{cov}\left(r_\mu, \overline{Q - Q_\nu}|_\nu\right). \quad (\text{A8})$$

## References

- [1] P. F. Smith and J. D. Lewin, *Phys. Rep.* **187**, 203 (1990).
- [2] J. D. Lewin and P. F. Smith, *Astropart. Phys.* **6**, 87 (1996).
- [3] G. Jungman, M. Kamionkowski and K. Griest, *Phys. Rep.* **267**, 195 (1996).
- [4] G. Bertone, D. Hooper and J. Silk, *Phys. Rep.* **405**, 279 (2005).
- [5] M. Drees and C. L. Shan, *J. Cosmol. Astropart. Phys.* **0706**, 011 (2007).
- [6] C. L. Shan and M. Drees, [arXiv:0710.4296 \[hep-ph\]](#) (2007).
- [7] M. Drees and C. L. Shan, *J. Cosmol. Astropart. Phys.* **0806**, 012 (2008).
- [8] CDMS Collab., Z. Ahmed *et al.*, [arXiv:0912.3592 \[astro-ph.CO\]](#) (2009).
- [9] CRESST Collab., R. F. Lang *et al.*, *Astropart. Phys.* **33**, 60 (2010); CRESST Collab., J. Schmalzer *et al.*, *AIP Conf. Proc.* **1185**, 631 (2009).

- [10] E. Aprile and L. Baudis, for the XENON100 Collab., *PoS IDM2008*, 018 (2008).
- [11] EDELWEISS Collab., A. Broniatowski *et al.*, *Phys. Lett. B* **681**, 305 (2009); EDELWEISS Collab., E. Armengaud *et al.*, *Phys. Lett. B* **687**, 294 (2010).
- [12] CRESST Collab., R. F. Lang *et al.*, *Astropart. Phys.* **32**, 318 (2010).
- [13] Y. T. Chou and C. L. Shan, [arXiv:1003.5277 \[hep-ph\]](#) (2010).
- [14] C. L. Shan, Ph.D. Thesis, [arXiv:0707.0488 \[astro-ph\]](#) (2007).
- [15] K. Freese, J. Frieman and A. Gould, *Phys. Rev. D* **37**, 3388 (1988).
- [16] J. Engel, *Phys. Lett. B* **264**, 114 (1991).
- [17] C. L. Shan, *New J. Phys.* **11**, 105013 (2009).
- [18] <http://pisrv0.pit.physik.uni-tuebingen.de/darkmatter/amidas/>.
- [19] C. L. Shan, *AIP Conf. Proc.* **1200**, 1031 (2010); [arXiv:0910.1971 \[astro-ph.IM\]](#) (2009).
- [20] L. Baudis, [arXiv:0711.3788 \[astro-ph\]](#) (2007).
- [21] M. Drees and G. Gerbier, contribution to “*The Review of Particle Physics 2008*”, C. Amsler *et al.*, *Phys. Lett. B* **667**, 1 (2008).
- [22] J. Gascon, [arXiv:0906.4232 \[astro-ph.HE\]](#) (2009).